Atmos. Chem. Phys. Discuss., 12, 17703–17721, 2012
www.atmos-chem-phys-discuss.net/12/17703/2012/
doi:10.5194/acpd-12-17703-2012

Atmospheric Chemistry and Physics Discussions

Lifetime and production rate of NO_x in the upper stratosphere and lower mesosphere in the polar spring/summer after the solar proton event in October–November 2003

F. Friederich[1], T. von Clarmann[1], B. Funke[2], H. Nieder[1], J. Orphal[1], M. Sinnhuber[1], G. P. Stiller[1], and J. M. Wissing[3]

[1]Karlsruhe Institute of Technology, Institute for Meteorology and Climate Research, Karlsruhe, Germany
[2]Instituto de Astrofísica de Andalucía, CSIC, Granada, Spain
[3]FB Physik, University of Osnabrück, Osnabrück, Germany

Received: 22 May 2012 – Accepted: 26 June 2012 – Published: 18 July 2012

Correspondence to: F. Friederich (felix.friederich@kit.edu)

Published by Copernicus Publications on behalf of the European Geosciences Union.

Abstract

We present altitude dependent lifetimes of NO_x, determined with MIPAS/ENVISAT, for the southern polar region after the solar proton event in October–November 2003. Varying in latitude and decreasing in altitude they range from about two days at 64 km to about 20 days at 44 km. The lifetimes are controlled by transport, mixing and photolysis. We infer dynamical lifetimes by comparison of the observed decay to photolytical lifetimes calculated with the SLIMCAT 3-D Model. Photochemical loss contributes to the observed NO_x depletion by 10 % at 44 km, increasing with altitude to 35 % at 62 km at a latitude of –63° S. At higher latitudes, the contribution of photochemical loss can be even more important.

In addition, we show the correlation of modeled ionization rates and observed NO_x densities under consideration of the determined lifetimes of NO_x, and calculate altitude dependent effective production rates of NO_x due to ionization. For that we compare ionization rates of the AIMOS data base with the MIPAS measurements for the whole Austral polar summer 2003/04. We derive effective NO_x-production rates to be applied to the AIMOS ionization rates which range from about 0.2 NO_x-molecules per ion pair at 44 km to 0.9 NO_x-molecules per ion pair at 54 km at a latitude of –63° S. At –73° S, the NO_x-production rate ranges from about 0.2 NO_x-molecules per ion pair at 44 km to 1.0 NO_x-molecules per ion pair at 60 km. These effective production rates are considerably lower than predicted by box model simulations which could hint at an overestimation of the modeled ionization rates.

1 Introduction

During the maximum of the 11-yr solar magnetic activity cycle, solar flares and coronal mass ejections (CME) are most frequent. During a CME, solar plasma is ejected into space, driving a shock front that can effectively accelerate particles. Propagating along the interplanetary field lines the energetic particles (protons, electrons and a few more

ACPD
12, 17703–17721, 2012

massive ions) may reach the Earth and precipitate – guided by the terrestrial magnetic field – in the polar cap regions where they cause ionization down to ~40 km altitude. This so-called Solar Proton/Particle Event (SPE) may also be followed by a geomagnetic storm as soon as the CME hits the geomagnetic field, forcing precipitation of low energetic particles and ionization in the upper atmosphere. Focussing on 42–62 km altitude we will concentrate mostly on the high-energetic particles from the SPE and their follow-ups: excitation, ionization, and dissociation of molecules. These particles have influence on the chemical composition, temperature, and dynamics of the Earth's atmosphere (e.g. Crutzen et al., 1975; Jackman et al., 2001, 2007).

According to Porter et al. (1976) 1.25 N-atoms are produced by each ion pair, partitioned in 0.55 $N(^4S)$ and 0.70 $N(^2D)$. $N(^4S)$ and $N(^2D)$ are also produced by

$$N^+ + O_2 \rightarrow O_2^+ + N(^4S,^2D) \quad \text{(R1)}$$

By the reactions

$$N(^4S) + O_2 \rightarrow NO + O \quad \text{(R2)}$$

$$N(^2D) + O_2 \rightarrow NO + O \quad \text{(R3)}$$

NO is produced. R3 is virtually immediate. Thus, models typically assume a production of NO and $N(^4S)$. NO is also produced directly by ionization, i.e. via:

$$NO^+ + X^- \rightarrow NO + X \quad \text{(R4)}$$

X^- denotes negative ions. At sunset NO is converted into NO_2 below 70 km:

$$NO + O_3 \rightarrow NO_2 + O_2 \quad \text{(R5)}$$

which reverts at sunrise to NO by:

$$NO_2 + h\nu \rightarrow NO + O \quad \text{(R6)}$$

NO can also be dissociated by photolysis:

$$NO + h\nu\ (< 191\,\text{nm}) \rightarrow N + O \quad \text{(R7)}$$

ACPD
12, 17703–17721, 2012

The predominant process of decomposition of NO_x (N, NO, NO_2) is:

$$N(^4S) + NO \rightarrow N_2 + O, \quad \text{(R8)}$$

which occurs in the stratosphere and lower mesosphere during the daytime because $N(^4S)$ is produced by photolysis, in competition to Reaction (R2).

The impact of the so-called Halloween SPE on NO_x in October–November 2003 has been investigated in a few studies (Seppälä et al., 2004, 2007; Jackman et al., 2005; López-Puertas et al., 2005; Baumgaertner et al., 2010; Funke et al., 2011). The lifetime of NO_x is typically a few days at altitudes from 44 km to 64 km (Brasseur and Solomon, 2005). So the multitude of MIPAS/ENVISAT measurements per day allows to determine the lifetime of NO_x in the middle atmosphere impacted by a SPE. We analyze these lifetimes in a first step (Sect. 3.1). With these altitude and latitude dependent lifetimes available, the dependence of the NO_x production on the ion production rate is estimated (Sect. 3.2). Since the downward transport of upper atmospheric air into the upper stratosphere and lower mesosphere has a huge impact on NO_x in the winter hemisphere, data of the Southern Hemisphere is analyzed (Siskind and Russell, 1996; Funke et al., 2005b; Randall et al., 2007). We compare our results to different studies which have also estimated the ion production rate in Sect. 4.

Ionization rates are provided by the Atmospheric Ionization Module Osnabrück (AIMOS). Data of MIPAS are described in Sect. 2.1, AIMOS is described in Sect. 2.2. Data analysis is shown in Sect. 3.

2 Used data

In this section, we describe the data used for this study. Mixing ratios of NO and NO_2 are retrieved from spectra of MIPAS (Sect. 2.1) and the 3-D model AIMOS is used to get ionization rates (Sect. 2.2).

ACPD
12, 17703–17721, 2012

2.1 MIPAS/ENVISAT

The Michelson Interferometer for Passive Atmospheric Sounding (MIPAS, Fischer et al., 2008) on the European Environment Satellite (ENVISAT) has recorded emission limb spectra since 2002. ENVISAT has a sun-synchronous orbit with an inclination of 98° at an altitude of about 800 km (783 km since 2010). All latitudes up to ±90° can be observed both at day and at night at about 10 a.m. and 10 p.m. local time, respectively. We use NO_x-data of the nominal measurement mode (Funke et al., 2005a), which covers altitudes from 6 km–68 km. MIPAS records limb emission spectra in the infrared wave range (4.1 µm–14.7 µm). The NO fundamental band at 5.3 µm and the NO_2 fundamental ν_3 band at 6.2 µm are used to determine the volume mixing ratio (vmr) profiles of NO and NO_2. Additional quantities available from the retrieval for each geolocation are the temperature T [K], the pressure p [hPa], volume mixing ratio and the averaging kernel (avk).

We used version V3O_NO_14 and V3O_NO2_13/14 which has substantially improved with respect to the retrieval setup described in Funke et al. (2005a) by (i) the use of log(vmr) instead of vmr in the retrieval vector, (ii) a revised correction scheme for line of sight variations of the NO_x partitioning close to the terminator, and (iii) joint-fitted vmr horizontal gradients at constant longitudes and latitudes.

In the analysis, we average vmr and the number density n over time and latitude bands. We only take $\overline{\text{vmr}}$ and $\overline{n}$ into account, when the arithmetic mean of the avk diagonal elements $\overline{\text{avd}}$ is greater than 0.03.

2.2 AIMOS

The Atmospheric Ionization Module Osnabrück, (AIMOS, Wissing and Kallenrode, 2009) is a 3-D model, which determines the atmospheric ionization caused by protons, electrons, and alpha particles. It is based on flux measurements of GOES (Geostationary Operational Environmental Satellite) and POES (Polar Operational Environmental Satellite) covering an energy range of 150 eV to 500 MeV for protons, 4 MeV to

ACPD
12, 17703–17721, 2012

500 MeV for alpha particles, and 150 eV to 2.5 MeV for electrons. In addition, the energy range of the electrons is extrapolated to 5 MeV. AIMOS provides ionization rates from 2002 until 2010, which depend on altitude, latitude and longitude. The spatial resolution is 3.6° × 3.6° with 67 pressure levels, ranging from 10^5 Pa to 1.7×10^{-5} Pa. The temporal resolution is two hours. The unit of the ionization rates is IPP $\mathrm{cm}^{-3}\,\mathrm{s}^{-1}$, IPP denotes ion pair production.

3 Data analysis

This section presents the procedure of the data analysis used for our investigation. The determinations of the lifetimes and the dependence of NO_x on the ion pair production (IPP) are shown in Sects. 3.1 and 3.2, respectively.

3.1 Lifetime of NO_x

The SPE in October–November 2003 induced a large increase of the NO_x vmr in polar latitudes above ~45 km which was observed, e.g. by MIPAS on ENVISAT (López-Puertas et al., 2005). The volume mixing ratio of NO_x has its maximum on 30 October. Subsequently, there is a decrease lasting for four days. We average MIPAS data of each retrieved altitude separately (42 km, 43 km, 44 km, 45 km, 46 km, 47 km, 48 km, 49 km, 50 km, 52 km, 54 km, 56 km, 58 km, 60 km, 62 km, and 64 km) and within latitude bins (±4°) over a time-period of six hours to get a smoothed vmr gradient. Then we fit an exponential function

$$\mathrm{vmr}(t) = \mathrm{vmr}(t_0) \cdot \exp\left(-\frac{t - t_0}{\tau}\right) + \mathrm{const.} \quad (1)$$

to the data after the maximum of vmr. t_0 denotes the time of the maximum of vmr. τ is the lifetime of NO_x, which depends on latitude and altitude. Consequently, the fit has three degrees of freedom (vmr(t_0), τ, const). Figure 1 shows 6 h-averaged MIPAS

ACPD
12, 17703–17721, 2012

measurements with the standard error of the mean (error bars) at an altitude of 62 km and at a latitude of $-73^{\circ} \pm 4^{\circ}$. The exponential fit to the data vmr(t) is computed by weighting each value with its inverse variance. τ and the 1σ-range of τ are shown in Fig. 2 (left) for all altitudes at latitudes of $-63^{\circ} \pm 4^{\circ}$ (top) and $-73^{\circ} \pm 4^{\circ}$ (bottom). The corresponding reduced χ^2 values between measurement and fit are shown on the right. They vary between 0 and 1.5. χ^2 values lower than one show on the one hand that the assumption of an exponential decay is reasonable. On the other hand they are an evidence that the standard error of the mean is overestimated by using the familiar estimator function (Toohey et al., 2011). The higher χ^2 becomes the more likely the fit is outside the error bars of some values.

The lifetime as calculated from MIPAS data depends on the altitude- and latitude-dependent photolysis rate and on a dynamic part due to horizontal transport and mixing. Vertical advection is small in polar summer. Horizontal transport and mixing are responsible for a distribution of NO_x towards latitudes outside the polar cap. In our idealized assumption, the source of NO_x is inside the polar caps due to the SPE and there is no NO_x enhancement outside the polar caps nor any important NO_x production during the three days after the SPE. So we can assume an exponential decay not only for the loss due to photolysis but also for dilution due to dynamics. The following relation applies to the combined lifetime:

$$\frac{1}{\tau} = \frac{1}{\tau_{\text{phot}}} + \frac{1}{\tau_{\text{dyn}}}. \quad (2)$$

The photolytic lifetimes τ_{phot} have been calculated by the SLIMCAT 3-D Model (Chipperfield, 1999) for the corresponding time and geolocations of the observations. The lifetime τ, the photolytic lifetime τ_{phot}, and the dynamic lifetime τ_{dyn} are displayed in Fig. 2 (left) depending on the altitude at latitudes of $-63^{\circ} \pm 4^{\circ}$ (top) and $-73^{\circ} \pm 4^{\circ}$ (bottom). The lifetimes τ, τ_{phot}, and τ_{dyn} decrease with increasing altitude. At a latitude of $-63^{\circ} \pm 4^{\circ}$ and at 44 km τ is 16.6 ± 5.0 days and it decreases to the highest analyzed altitude at 64 km where it is only 2.4 ± 0.5 days. At a latitude of $-73^{\circ} \pm 4^{\circ}$ and at 44 km

ACPD
12, 17703–17721, 2012

τ is 14.4 ± 5.0 days and it decreases to the highest analyzed altitude at 64 km where it is only 2.3 ± 0.6 days. The errors specify the 1σ-range.

The photochemical loss becomes more important with increasing altitude. At a latitude of $-63^\circ \pm 4^\circ$ and at an altitude of 44 km the photolysis rate $J = \frac{1}{\tau_{\text{phot}}}$ is 10 % of $\frac{1}{\tau}$, at 62 km J is already at 35 %. At a latitude of $-73^\circ \pm 4^\circ$, photolysis is the main process between the altitude range of 49 km and 54 km.

3.2 Dependence of NO_x on ion pair production

With estimates of NO_x lifetimes available we can now analyze the relation between the number density n of NO_x and the ion production rate due to the particle precipitation. n is calculated from the retrieved quantities T, p, and vmr. It is intended to reproduce a dependence of n on ion pair production. First we should mention, that polar winter descent of thermospheric air entails a limitation in analyzing data in the winter hemisphere. That air intrudes in the mesosphere and elevates the vmr of NO_x about some orders of magnitude through the EEP Indirect Effect (Siskind and Russell, 1996; Funke et al., 2005b; Randall et al., 2007). Smaller enhancements due to the SPE impact cannot be easily distinguished from the descending NO_x-rich air masses. Therefore we do not analyze the northern winter hemisphere.

Considering that, data of MIPAS measurements of southern polar latitudes of the Austral summer 2003/04 are used at altitudes from 44 km to 62 km. The number density is averaged every 6 h over 24 h. There should be a dependence of the enhancement of the NO_x-number density to the ion production rate, because of NO_x-production due to ionization. In addition, the temporal evolution of NO_x is modulated by the lifetime τ of a NO_x-molecule. In the following, the production of NO_x due to ionization will be described using MIPAS data. The difference of the number density of NO_x affected by ion pair production (IPP) due to energetic partical precipitation $n(\text{IPP}, t_0)$ and the backround number density $n(\text{IPP} = 0, t_0)$ without particle precipitation at the time t_0 is:

$$\Delta n_{\text{MIPAS}}(t_0) = n(\text{IPP}, t_0) - n(\text{IPP} = 0, t_0). \quad (3)$$

ACPD
12, 17703–17721, 2012

Consequently, $\Delta n_{\mathrm{MIPAS}}(t_0)$ denotes the enhancement of n due to IPP. $n(\mathrm{IPP}, t_0)$ can be determined by analyzing MIPAS data. $n(\mathrm{IPP}=0, t_0)$ is determined by means of a polynomial function, fitted to the MIPAS data of the Austral summer 2003/04. Both $n(\mathrm{IPP}, t_0)$ and $n(\mathrm{IPP}=0, t_0)$ are shown in Fig. 3 (left) as crosses (the color code is time dependent) and as a green graph, respectively, for a latitude of $-73^\circ \pm 4^\circ$ and at an altitude of 56 km.

The enhancement of the number density of NO_x at the time t_0 can also be determined theoretically by assuming a production rate of 1.25 $\frac{NO_x}{\text{ion pair}^{-1}}$. The time dependence of $\Delta n_{\mathrm{theory}}$ can thus be determined as below:

$$\Delta n_{\mathrm{theory}}(t_0) = 1.25 \cdot \int_{-\infty}^{t_0} \mathrm{IPP}(t) \cdot e^{-\frac{t_0 - t}{\tau}} \mathrm{d}t. \quad (4)$$

This equation describes the NO_x enhancement $\Delta n_{\mathrm{theory}}$ at any time t_0 as the accumulated surviving part of NO_x production. The AIMOS database (Sect. 2.2) provides IPP(t), τ was determined in Sect. 3.1. The integral is signified by

$$I(\mathrm{IPP}, \tau, t_0) = \int_{-\infty}^{t_0} \mathrm{IPP}(t) \cdot e^{-\frac{t_0 - t}{\tau}} \mathrm{d}t. \quad (5)$$

In Fig. 3 (right), $\Delta n_{\mathrm{MIPAS}}(t_0)$ is plotted over $I(\mathrm{IPP}, \tau, t_0)$ at a latitude of $-73^\circ \pm 4^\circ$ and at an altitude of 56 km. It reveals, as expected, that $\Delta n_{\mathrm{MIPAS}}(t_0)$ increases with $I(\mathrm{IPP}, \tau, t_0)$. Up to the the value $I = 5 \times 10^7 \frac{1}{\mathrm{d \cdot cm^3}}$ it seems that there are two branches. The branch at which the gradient is observable is caused by the SPE and the subsequent decrease of n. The lower branch represents the other days, especially the day before the SPE (yellow crosses). At these days the ion pair production inreases, n does not, however. This means that AIMOS shows enhanced ionization rates on 28 October, but MIPAS does not show enhanced NO_x volume mixing ratios. There is another noticeable

ACPD
12, 17703–17721, 2012

discrepancy regarding the NO_x-enhancement after 20 November. Either the effective production rate of NO_x is higher under the certain conditions of the 20 November or there is a disagreement between the two data sets. The red curve represents the theoretical trend with an effective NO_x-production rate of 1.25. The green curve represents the relation described by Eq. (4) with a scalar x replacing the theoretical value of 1.25 which has been fitted to the distribution. x is the empirically determined production rate of NO_x per ion pair and is altitude dependent. These altitude dependent production rates are shown in Fig. 4 (left). The green error bars show the 1-σ uncertainties of the empirically determined NO_x production rates per ion pair x. The altitude dependent χ^2 value of the fits is shown in the right-hand figures. Most of the χ^2 values are significantly larger than one and so they argue for a non-linear NO_x-production. The NO_x-production rate is significantly lower than 1.25 at all altitudes. This is obvious, because N(^{4}S) not only produces NO (Reaction R2) but also destroys NO (Reaction R8). The black and red curves represent theoretical values of the effective NO_x-production rate and are explained in Sect. 4.3.

4 Comparison with previous model studies

Hereafter, the results from Sect. 3.2 are compared with different model studies, cited in the title of each subsection.

4.1 Jackman et al. (2005)

Jackman et al. (2005) used the Goddard Space Flight Center (GSFC) 2-D atmospheric model and measurements of the Halogen Occultation Experiment (HALOE) on the Upper Atmosphere Research Satelitte (UARS) to study the Halloween SPE. The GSFC 2-D model accounts for the proton flux, measured by the Geostationary Operational Environmental Satellites (GOES) 11, but neither for the alpha particle flux nor for the electron flux. The model uses the nitrogen-production of Porter et al. (1976) as described

ACPD
12, 17703–17721, 2012

above. To model the NO_x -change, the authors examined the difference of a "perturbed" (with ionization rates of a SPE) and an "unperturbed" model run. To quantify the observed NO_x change, the authors examined the difference of the days after 30 October and the "backround" from 12–15 October. The production of the GSFC 2-D model fits very well to the HALOE-measurement, but between 50 km and 60 km it seems to be a little too high.

4.2 Baumgaertner et al. (2010)

As in the study before, Baumgaertner et al. (2010) only accounted for the proton flux, measured by GOES. In a first run, they start with a production rate of 0.55 N(^{4}S) and 0.7 N(^{2}D), resulting in the production of NO, per ion pair. Results of the ECHAM/MESSy Atmospheric Chemistry (EMAC) model are compared with measurements of MIPAS. The mesospheric enhancement of NO_2 is lower in the measurement (50 ppbv) than in the simulation (60 ppbv). However, the difference can be explained by systematic errors and dynamical effects. In order to improve the simulated N_2O abundance, which is seven times higher than the measured one, tests with alternative altitude dependent N- and NO-production rates (each between 0 and 1.2) were performed. They present in Fig. 9 of Baumgaertner et al. (2010) the NO-production rates, which fitted best. Their NO-production rates are about three times higher at altitudes from 42 km to 50 km, 20 % higher at 54 km and significantly lower from 58 km to 66 km than the NO_x-production rates at a latitude of $-63^\circ \pm 4^\circ$ from Fig. 4 (top).

4.3 Funke et al. (2011)

In the High Energy Particle Precipitation in the Atmosphere (HEPPA) intercomparison the ability of numerous models to simulate atmospheric composition changes after the Halloween SPE was investigated (Funke et al., 2011). All involved models show a NO_y increase between 1.5 hPa and 0.4 hPa (~45 km–55 km), which is systematically higher than the increase measured by MIPAS. The authors give two different reasons for that.

ACPD
12, 17703–17721, 2012

First, the ionization rates provided by AIMOS may be too high for these altitudes. At these altitudes, uncertainties of the measurements of the electrons with an energy range of 300 keV–2.5 MeV and the extension to 5 MeV based on these measurements are rather high. Also, models using a family approach for NO_x tend to overestimate the net NO_x production. Reaction (R2) strongly depends on temperature and the initial NO_y abundance. To demonstrate this, the authors show the production rate efficiency of NO_x (ratio of the net NO_x increase and the integrated initial N production) for the Northern Hemisphere during 28 October–1 November determined by a box model. We used the same box model, to test the dependence of the effective production. But we used other initial values for the Southern Hemisphere namely temperature, NO, NO_2, O_3, measured by MIPAS, the ionisation rates of AIMOS and the photolysis rates of SLIMCAT. In Fig. 4 (left) the black curve shows the result of this box model. The red curves show the estimated error range after varying the initial values (temperature: ±10 K and NO, NO_2, O_3: ±10 %). The shape of the black curve is explained by two effects. First, Reaction (R2) is strongly temperature dependent. It is less effective in colder and therefore higher altitudes in the mesosphere. Additionally, the photolysis rate of NO increases with altitude. At –63° and –73° S the effective NO_x-production rates of the box model are considerably higher from 44 km to 52 km. At higher altitude the error bars of the measured and modeled effective NO_x-production rates overlap at –63° S. At –73° S the modeled values are higher at 60 km and 62 km.

5 Conclusions

We showed a simple method to derive lifetimes of NO_x after a solar proton event by means of MIPAS measurements. The lifetime of NO_x at that time at altitudes between 44 km and 64 km mainly depends on dynamic effects and less on photolysis, because in most cases the lifetime of NO_x is significantly shorter than the sole photolytic lifetime. Including the lifetime of NO_x, we were able to present the dependence of the NO_x-production on the ion pair production.

ACPD
12, 17703–17721, 2012

The calculated NO_x-production rates do not reproduce the theoretical value of 1.25 due to chemical and photochemical loss processes of NO_x.

The measured production rates are outside the error bars and significant lower than in the box model of Funke et al. (2011) at altitudes between 44 km and 52 km. At the same altitudes, the models of the HEPPA intercomparison show a too high NO_x-production. One reason could be that the measurement of precipitating energetic electrons has significant errors and may result in too high ionization rates at these altitudes.

Acknowledgements. F. Friederich, H. Nieder, and M. Sinnhuber gratefully acknowledge funding by the Helmholtz society, grant VH-NG-624.

References

Baumgaertner, A. J. P., Jöckel, P., Riese, H., Stiller, G., and Funke, B.: Energetic particle precipitation in ECHAM5/MESSy – Part 2: Solar proton events, Atmos. Chem. Phys., 10, 7285–7302, doi:10.5194/acp-10-7285-2010, 2010. 17706, 17713

Brasseur, G. P. and Solomon, S.: Aeronomy of the Middle Atmosphere, 3rd edn., Springer, Dordrecht, The Netherlands, 2005. 17706

Chipperfield, M. P.: Multiannual simulations with a three-dimensional chemical transport model, J. Geophys. Res., 104, 1781–1805, 1999. 17709

Crutzen, P. J., Isaksen, I. S. A., and Reid, G. C.: Solar proton events – stratospheric sources of nitric oxide, Science, 189, 457–459, doi:10.1126/science.189.4201.457, 1975. 17705

Fischer, H., Birk, M., Blom, C., Carli, B., Carlotti, M., von Clarmann, T., Delbouille, L., Dudhia, A., Ehhalt, D., Endemann, M., Flaud, J. M., Gessner, R., Kleinert, A., Koopman, R., Langen, J., López-Puertas, M., Mosner, P., Nett, H., Oelhaf, H., Perron, G., Remedios, J., Ridolfi, M., Stiller, G., and Zander, R.: MIPAS: an instrument for atmospheric and climate research, Atmos. Chem. Phys., 8, 2151–2188, doi:10.5194/acp-8-2151-2008, 2008. 17707

Funke, B., López-Puertas, M., von Clarmann, T., Stiller, G. P., Fischer, H., Glatthor, N., Grabowski, U., Höpfner, M., Kellmann, S., Kiefer, M., Linden, A., Mengistu Tsidu, G., Miliz, M., Steck, T., Stiller, G. P., Wang, D. Y.: Retrieval of stratospheric NO_x from 5.3 and 6.2 µm nonlocal thermodynamic equilibrium emissions measured by Michelson Interferome-

ACPD

12, 17703–17721, 2012

ter for Passive Atmospheric Sounding (MIPAS) on Envisat, J. Geophys. Res., 110, D09302, doi:10.1029/2004JD005225, 2005a. 17707

Funke, B., López-Puertas, M., Gil-López, S., von Clarmann, T., Stiller, G. P., Fischer, H., and Kellmann, S.: Downward transport of upper atmospheric NO_x into the polar stratosphere and lower mesosphere during the Antarctic 2003 and Arctic 2002/2003 winters, J. Geophys. Res., 110, D24308, doi:10.1029/2005JD006463, 2005b. 17706, 17710

Funke, B., Baumgaertner, A., Calisto, M., Egorova, T., Jackman, C. H., Kieser, J., Krivolutsky, A., López-Puertas, M., Marsh, D. R., Reddmann, T., Rozanov, E., Salmi, S.-M., Sinnhuber, M., Stiller, G. P., Verronen, P. T., Versick, S., von Clarmann, T., Vyushkova, T. Y., Wieters, N., and Wissing, J. M.: Composition changes after the "Halloween" solar proton event: the High Energy Particle Precipitation in the Atmosphere (HEPPA) model versus MIPAS data intercomparison study, Atmos. Chem. Phys., 11, 9089–9139, doi:10.5194/acp-11-9089-2011, 2011. 17706, 17713, 17715

Jackman, C. H., McPeters, R. D., Labow, G. J., Fleming, E. L., Praderas, C. J., and Russell, J. M.: Northern Hemisphere atmospheric effects due to the July 2000 solar proton event, Geophys. Res. Lett., 28, 2883–2886, 2001. 17705

Jackman, C. H., DeLand, M. T., Labow, G. J., Fleming, E. L., Weisenstein, D. K., Ko, M. K. W., Sinnhuber, M., and Russell, J. M.: Neutral atmospheric influences of the solar proton events in October–November 2003, J. Geophys. Res., 110, A09S27, doi:10.1029/2004JA010888, 2005 17706, 17712

Jackman, C. H., Roble, R. H., and Fleming, E. L.: Mesospheric dynamical changes induced by solar proton events in October–November 2003, Geophys. Res. Lett., 34, L04812, doi:10.1029/2006GL028328, 2007. 17705

López-Puertas, M., Funke, B., Gil-López, S., von Clarmann, T., Stiller, G. P., Höpfner, M., Kellmann, S., Fischer, H., and Jackson, C. H.: Observations of NO_x-enhancements and ozone depletion in the Northern and Southern Hemispheres after the October–November 2003 solar proton events, J. Geophys. Res., 110, A09S44, doi:10.1029/2005JA011051, 2005. 17706, 17708

Porter, H. S., Jackman, C. H., and Green, A. E. S.: Efficiencies for production of atomic nitrogen and oxygen by relativistic proton impact in air, J. Chem. Phys., 65, 154–167, doi:10.1063/1.432812, 1976. 17705, 17712

Randall, C. A., Harvey, V. L., Singleton, C. S., Bailey, S. M., Bernath, P. F., Codrescu, M., Nakajima, H., and Russell III, J. M.: Energetic particle precipitation effects on the

ACPD
12, 17703–17721, 2012

Southern Hemisphere stratosphere in 1992–2005, J. Geophys. Res., 112, D08308, doi:10.1029/2006JD007969, 2007. 17706, 17710

Seppälä, A., Verronen, P. T., Kyrölä, E., Hassinen, S., Backman, L., Hauchecorne, A., Bertaux, J. L., and Fussen, D.: Solar proton events of October–November 2003: ozone depletion in the Northern Hemisphere polar winter as seen by GOMOS/Envisat, Geophys. Res. Lett., 31, L19107, doi:10.1029/2004GL021042, 2004. 17706

Seppälä, A., Cliverd, M. A., and Rodger, C. J.: NO_x enhancements in the middle atmosphere during 2003–2004 polar winter: relative significance of solar proton events and the aurora as a source, J. Geophys. Res., 112, D23303, doi:10.1029/2006JD008326, 2007. 17706

Siskind, D. E. and Russell III, J. M.: Coupling between middle and upper atmospheric NO: constraints from HALOE observations, Geophys. Res. Lett., 27, 329–332, doi:10.1029/1999GL010940, 1996. 17706, 17710

Toohey, M., von Clarmann, T., Hegglin, M., Tegtmeier, S., and the SPARC Data Initiative team: SPARC Data Initiative: climatology uncertainty assessment, World Climate Research Programme, Open Science Conference, Denver, 2011. 17709

Wissing, J. M. and Kallenrode, M.-B.: Atmospheric Ionization Module Osnabrück (AIMOS): a 3-D model to determine atmospheric ionization by energetic particles from different populations, J. Geophys. Res., A06104, doi:10.1029/2008JA013884, 2009. 17707

ACPD
12, 17703–17721, 2012

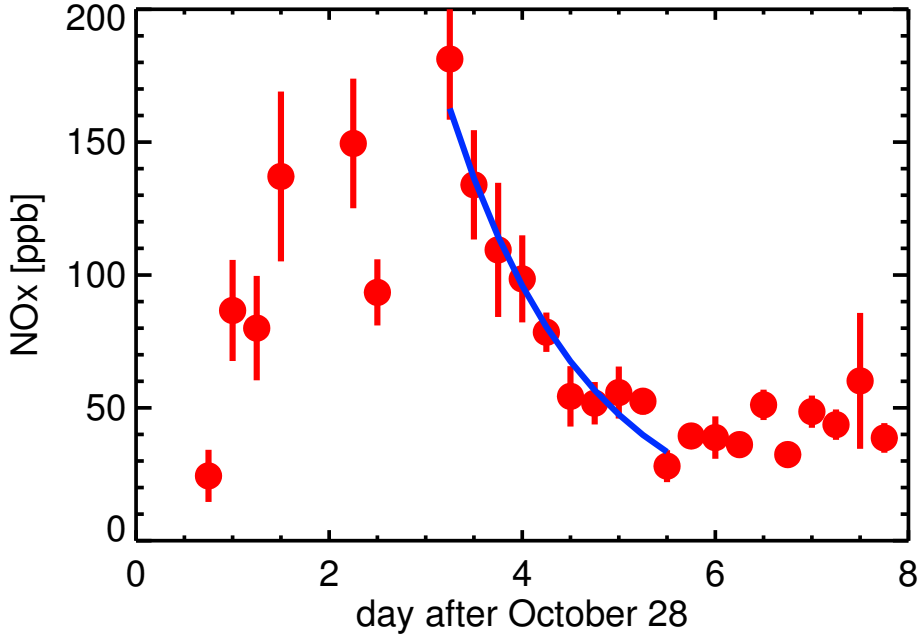

Fig. 1. MIPAS vmr measurements of NO_x (red) at October–November 2003 and a fit of an exponential function (blue) at an altitude of 62 km and at a latitude of $-73^\circ \pm 4^\circ$. The error bars show the error of the mean of the zonal averages.

ACPD
12, 17703–17721, 2012

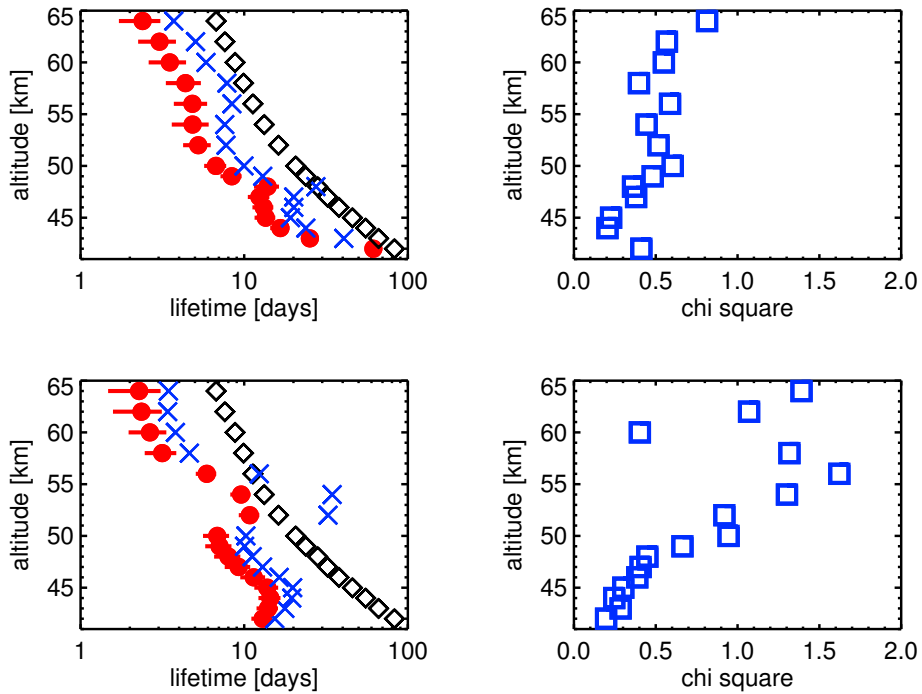

Fig. 2. Left: altitude dependent lifetimes of NO_x after the SPE at 30 October at latitudes of $-63^\circ \pm 4^\circ$ (top) and $-73^\circ \pm 4^\circ$ (bottom). The lifetimes τ as calculated from MIPAS measurements are displayed in red. The red error bars show the 1σ-range of the value. The photolytic lifetimes τ_{phot} taken from SLIMCAT are displayed in black diamonds. The resulting dynamic lifetimes τ_{dyn} are diplayed in blue crosses. Right: altitude dependent χ^2 values between measurement and fit of the exponential function at the latitudes $-63^\circ \pm 4^\circ$ (top) and $-73^\circ \pm 4^\circ$ (bottom) according to the figures left.

ACPD
12, 17703–17721, 2012

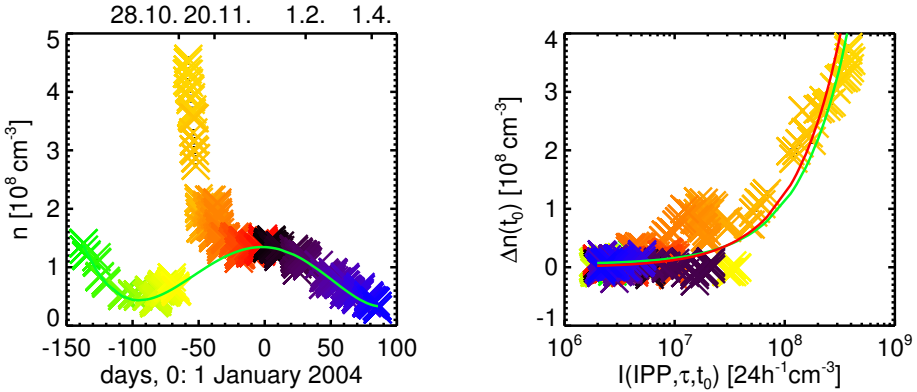

Fig. 3. Left: time curve of the number density n of NO_x at a geomagnetic latitude of $-73^\circ \pm 4^\circ$ and at an altitude of 56 km in the Austral summer 2003/04. The color code shows the time dependence. The green curve is a fitted polynomial function and shows the backround number density n(IPP = 0). Right: Δn_{MIPAS} (the difference of the number density and the correspondent value of the fitted function at the plot left) is plotted in dependence of $I(\mathrm{IPP}, \tau, t_0)$, specified in Eq. (5), at a geomagnetic latitude of $-73^\circ \pm 4^\circ$ and at an altitude of 56 km. The color code is the same as in the figure left. The green curve is a linear fit. The red curve shows the theoretical function for a production rate of 1.25 N per ion pair. In both plots the standard error of the mean is shown by black error bars.

ACPD
12, 17703–17721, 2012

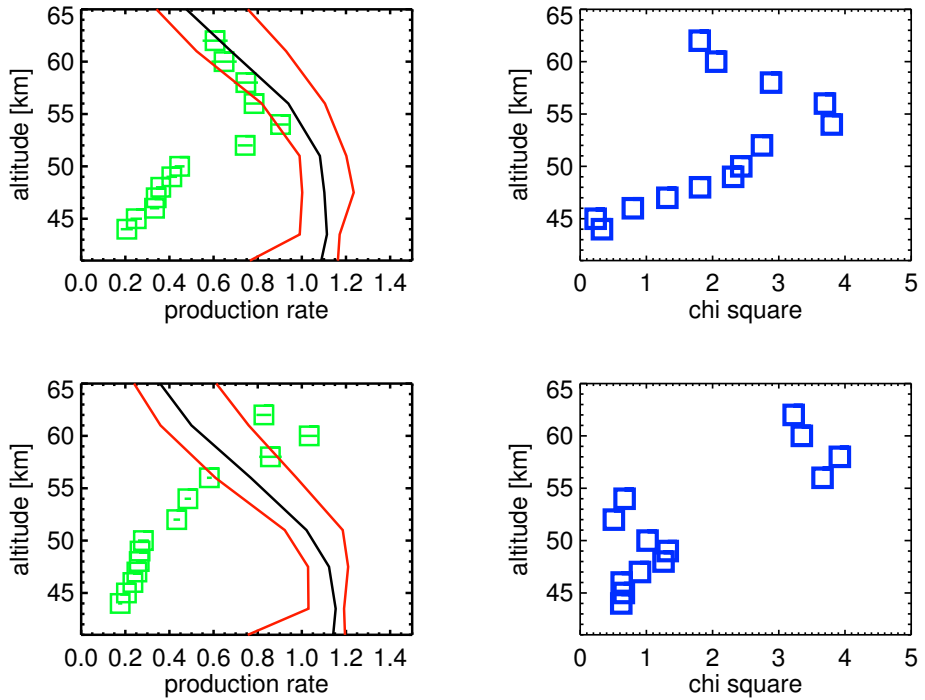

Fig. 4. Left: number of the produced NO_x-molecules per ion pair x in dependence of the altitude at a geomagnetic latitude of $-63^\circ \pm 4^\circ$ (top) and $-73^\circ \pm 4^\circ$ (bottom). The production rate per ion pair x is the gradient of the fit shown as green line in Fig. 3 (right panel). The error bars show the 1-σ range of the production rate. The black curve shows the effective daytime NO_x-production rate per ion pair, calculated with a box model. The red curves show the error range after varying the initial values of this box model as described in Sect. 4.3. Right: altitude-dependent χ^2 value of the fits related to the green line in Fig. 3 (right panel).

ACPD
12, 17703–17721, 2012